IL NUOVO CIMENTO **42 C** (2019) 230
DOI 10.1393/ncc/i2019-19230-7

COMMUNICATIONS: SIF Congress 2018

The MEV project: A new high-resolution telescope for the Muography of Etna Volcano

G. GALLO([1])([2]) on behalf of the MEV PROJECT COLLABORATION

([1]) *Dipartimento di Fisica e Astronomia Ettore Majorana, Università di Catania Catania, Italy*
([2]) *INFN, Laboratori Nazionali del Sud - Catania, Italy*

received 23 August 2019

Summary. — The Muography of Etna Volcano (MEV) project aims at developing a high-resolution muon telescope for the muography of the summit area of the Etna volcano. A muon tracking telescope, based on plastic scintillation strips with WLS fibers embedded and photomultipliers readout, was built and tested during 2017. The telescope is composed of three 1×1 m^2 position sensitive planes and the total angular aperture is about $\pm 45^\circ$, with an angular resolution not exceeding 0.4 msr. During the design of the detector, a special effort was devoted to mechanics and electronics in order to build a detector able to face the harsh conditions at the top of a high mountain. This paper summarizes the features of the first telescope prototype already operating at the top of the Etna volcano and the results of the test phase which lasted from January to July 2017.

1. – Introduction

Muography, or muon-radiography, is a technique similar to the common X-ray radiography, where the role of the photons is taken by muons. These elementary particles, with a mass equal to about 200 times that of the electron, are continuously produced in the upper part of the atmosphere by the interaction of primary cosmic rays with the molecules of air. Being the muons highly penetrating particles, they can easily reach the Earth surface and be absorbed after traversing hundreds, or also thousands, of meters of soil or rock. In principle, it is possible to obtain a two-dimensional density map of the object traversed by muons from a measure of their absorbing rate, which enables to easily recognize areas of significantly different densities.

The interest on muography has rapidly grown during the last decades [1-7] because the promising results of this technique are strictly related to the mitigation of volcanic hazards, which relies on the capability to interpret surface observations in terms of subsurface processes that may suggest a volcano is breaking its equilibrium state. Nowadays

the monitoring of active volcanoes and also the investigation of their internal structure is performed by the use of different techniques, mainly based on the study of ground deformation, seismicity, gas emission and gravity. But these methods give access to reliable information on the processes that occur at greater depths, while they are not suited for the shallowest levels of volcanic plumbing system due to steep topography and a large number of fractures.

Muography and its potential to give information on the interior of large structures such as a volcano could be the keystone to address this issue. For a review of muon imaging techniques and their applications, see [8]. This is the scenario in which the MEV project was born with the first goal of realizing a muon telescope able to study the summit part of Etna [9]. Once the primary target is achieved, the purpose of this collaboration between physicists, engineers, geophysicist and volcanologists will be the construction of a permanent monitoring network of the active craters of the volcano by means of muon imaging. The use of more than one telescope to investigate the same object will allow to reconstruct a three-dimensional density map of the target, *i.e.*, a tomography.

2. – The MEV telescope

The quantity to be measured in order to realize a muography is the integral flux of muons by means of a telescope able to track the particles inside its field of view (FOV). The telescope works in transmission mode, *i.e.*, it is necessary that no other macroscopic object lies behind the target so that it will remain the unique cause of muon flux attenuation. A fundamental assumption in this context is that muons follows a straight path traversing the object, *i.e.*, Multiple Coulomb Scattering (MCS) can be neglected and the particle trajectory can be back-projected to reconstruct the linear path of the muons inside the target.

The first prototype of the MEV telescope was built at the Department of Physics and Astronomy "E. Majorana" of the University of Catania. It is based on three parallel X-Y position sensitive Logical Planes (LPs), with a sensitive area of $1\,\mathrm{m}^2$. Each logical plane is constituted by two physical planes of $N = 99$ scintillating bars with a nominal size of $1 \times 1 \times 100\,\mathrm{cm}$ aligned along X- or Y-direction respectively. The two outer LPs are placed 97 cm far away from each other and the third one lays in the middle. The scintillating strips are extruded plastic bars with a central 2.5 mm hole, through which two Wave Length Shifting (WLS) fibers are inserted to transport the photons to a Position Sensitive PhotoMultiplier (PSPM). The scintillating strips are coated by a white reflector on each external side. Figure 1 shows some photos taken during the construction of the telescope.

Each LP, therefore, has $2 \times N$ intersecting strips and $4 \times N$ optical channels, one for each WLS fiber. This number was minimized by the use of a channel reduction system, already employed in other detectors, see refs. [10, 11], which proves to be particularly useful for this application. Briefly, the two WLS fibers of each strip are differently routed: one WLS fiber is coupled with those of the same *Group*-set, while the other one is coupled with the fibers of the corresponding *Unit*-set, *i.e.*, the i-th fiber for each *Group*-set. For example, the fourth ($i = 4$) WLS fibers of every *Unit*-set are grouped together. In the MEV telescope each *Group* is composed by $n = 10$ strips, but this number can vary for the specific application. Combining the information of *Group*-set and *Unit*-set, the hit strip can be uniquely reconstructed, without any loss of information, and the total number of readout channels required is equal to 40 for each LP.

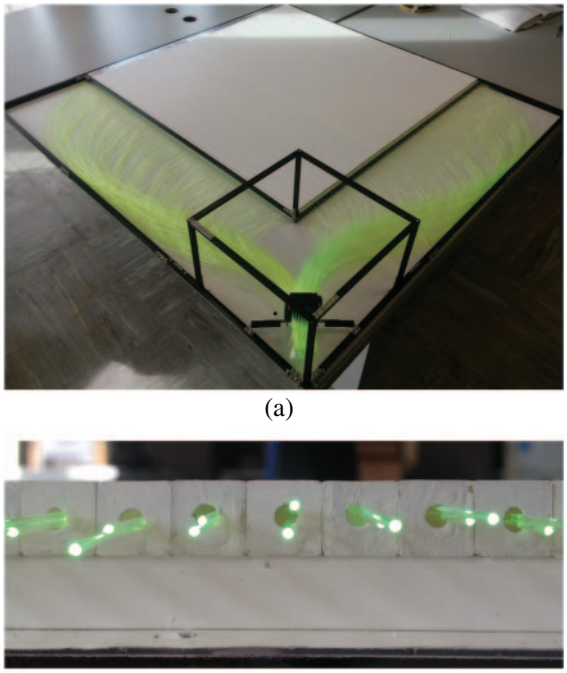

(a)

(b)

Fig. 1. – Assembly of a telescope position sensitive plane. Figure 1(a) shows on open LP with two layers of scintillation bars enclosed in an aluminum frame; fig. 1(b) is a detail of the WLS fibers embedded in each bar.

A LP of the telescope could be thought as a matrix of $N \times N$ pixels. The combination of all possible pixel pairs of the outer matrices establishes a set of $(2N-1)^2$ discrete directions of sight. The overall solid angle covered by a muon telescope based on scintillating strips and its angular resolution depend on the number of pixels, their size p ($p = 100/N$ cm) and the distance D between front and back matrices. The geometric characteristics, including the sensitive area of the MEV telescope, are summarized by the acceptance function $\mathcal{T}$ displayed in fig. 2 together with the angular resolution. For details on $\mathcal{T}$ definition, see ref. [12]. The maximum acceptance, corresponding to the direction perpendicular with respect to the LPs and passing through the center of the telescope sensitive area, is equal to about $1\,\mathrm{cm}^2\,\mathrm{sr}$, whereas the angular aperture is about $\pm 45°$ and the resolution does not exceed $4 \times 10^{-4}\,\mathrm{sr}$.

The MEV telescope was designed to be placed horizontally, *i.e.*, with its axis oriented perpendicular to the zenith, in such a way that the front of the detector faces the target object while the opposite side has no obstacles in front of it. The muon flux attenuated by the target can be measured simultaneously to the unaffected one (in the following referred as "open sky" flux) and, from a comparison of the two quantities, the transmission coefficient of muon flux through the object in study can be obtained.

2˙1. *Front-End and Read-Out electronics.* – Each LP has its custom designed Front-End (FE) board. The main components of a FE board are a 64 channels PSPM and a MAROC3 chip, which pre-amplifies and shapes the analog signal from the PSPM with

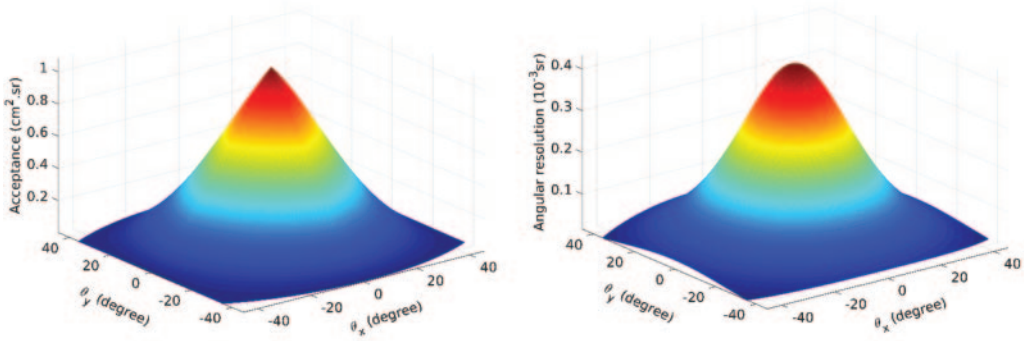

(a) (b)

Fig. 2. – Distribution of the telescope acceptance $\mathcal{T}$ (a) and angular resolution (b) for each discrete direction of sight of the MEV telescope ($N = 99$, $p \simeq 1.01\,\text{cm}, D = 97\,\text{cm}$). Both quantities are displayed as functions of azimuth θ_x and zenith angle θ_y. The telescope axis corresponds to $(\theta_x, \theta_y) = (0, 0)$. The plots were created using the MATLAB software.

a peak time of about 20 ns and compares all the signals to a common threshold, giving a digital time-over-threshold (ToT) signal for each channel. PSMSs were choosen as light sensors because they guaranteed a very low dark current and greater stability under temperature variations with respect to Silicon PhotoMultipliers (SiPMs) available at the time of detector construction (2016). Figure 3 shows an example of a FE board designed for the MEV telescope.

The output of the FE boards is acquired, filtered and processed by a System-on-Module (SOM), manufactured by National Instrument, on a single Read-Out (RO) board. The RO board, as the FE, is custom designed in order to meet all the requirements of the MEV project, first of all reliability, compactness and low power consumption. The FPGA embedded in the SOM could be easily programmed by means of LabVIEW, a software for test applications and control systems which offers a graphical approach. A scheme of the complete electronic chain is shown in fig. 4. Here another advantage of the channel reduction system is clearly visible, *i.e.*, the possibility to use a single SOM to

Fig. 3. – A front-end (FE) board equipped with a Hamamatsu H8500 64 channel PSPM and a MAROC3 chip.

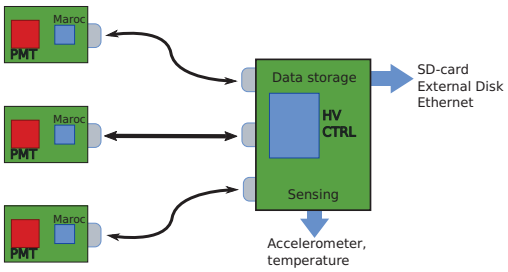

Fig. 4. – Diagram of the electronic chain of the telescope.

handle data coming from the three FE boards and ensure the synchronization between them.

Data are locally stored in a SD card memory. The management system of the detector is set to write a bunch of data in a progressively labeled file every ten minutes. The detector is equipped with a 4G LTE wireless router in order to send the data to a cloud storage at the Department of Physics when the network signal is available.

2˙2. *Mechanics and power supply.* – A cubic container with external side of about 1.5 m houses the aluminum frame which holds the LPs and the electronics aligned. The box has been designed to ensure light and water insulation of the detector and is mounted on a modular frame with adjustable legs to cope with terrain irregularities. Two solar panels (size: 150×80 cm; weight: 40 kg; output: 260 W, 12 A) are mounted on the roof of the box and they charge two batteries (12 V, 205 A h) housed inside the container. The total weight of the structure is about 300 kg and it requires a truck with a mechanical arm to be transported, but the inner structure of the detector is completely modular, so each LP (about 50 kg) can be carried by hands and the telescope can be assembled in field. This could be a solution for a short data taking campaign during summer, but the MEV telescope was designed to work in every climate condition.

3. – Test measurement campaign and running condition

The first prototype of the MEV telescope was installed at the facility of the National Institute for Geophysics and Volcanology (INGV) in the village of Nicolosi (13 km from Catania) for the test campaign. This phase started in January 2017 and ended in July of the same year. The effective time of data acquisition was about 103 days, considering short time periods of measurement interruption due to tuning and adjustment of the system. To demonstrate the correct functionality of the telescope, the goal of the test campaign was the muography of Monti Rossi, an extinct volcanic cone at a distance of about 900 m from the telescope location, as shown in fig. 5.

The trigger condition to start the record of an event is the presence of a X and a Y signal in each plane, within a time window of 80 ns. This compelling trigger condition —three two-fold coincidence— was chosen to filter out any signal generated by the very low dark current of the PSPMs. The SOM simultaneously samples at 200 MHz all 120 channels of the three LPs of the detector, so the output of an event consists of an array of 120×16 bits. In this context, "bit" is intended as a "binary word" that can be equal to 0 (low state) or 1 (high state). With reference to the data acquired by the MEV telescope, a bit is triggered in high state if the signal in the corresponding channel is higher than threshold.

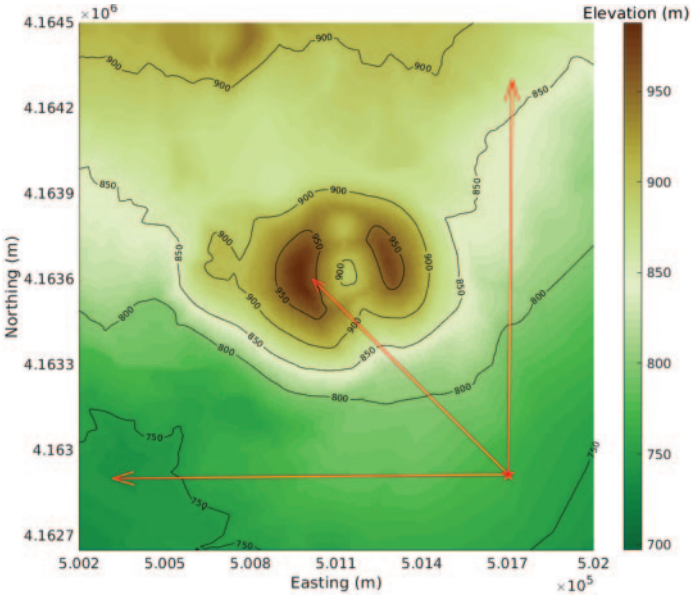

Fig. 5. – Contour map of the Monti Rossi zone, obtained from a 10 m Digital Elevation Model by INGV (2014). The red star marks the position of the telescope during the test phase and the arrows show its azimuthal field of view with the telescope axis in the middle.

In order to further reduce the spurious coincidences due to other sources of noise, an offline analysis was implemented in MATLAB. The main steps of this procedure for the reconstruction of an event are:

- All the hits from the possible combinations of *Group*-set and *Unit*-set are reconstructed for each LP. Events with more than 2 high *Group*-set bits are marked as noise.
- The hits on each LP are grouped by a clustering algorithm based on DBSCAN (Density-Based Spatial Clustering of Applications with Noise) popular method [13], with minimum number of points in a cluster equal to 1 and ε distance within neighbors belonging to the same cluster equal to $\sqrt{2}$ strips. Clusters which contain more than 4 hits are marked as noise. Events with more than 9 clusters on any LP are marked as noise.
- For non-noisy events, the cluster centers are calculated and a 3D linear fit algorithm checks that the reconstructed centers —one on each LP— match a linear trajectory, discarding the non-aligned ones. An exhaustive description of the linear fit algorithm can be retrieved in [9].

The cuts on maximum number of high *Group*-set bits, cluster size and number of clusters were chosen considering a particle that crosses a logical plane at the intersection between two adjacent X- and Y-*Group*-set, which produces 2 X- and 2 Y- high *Group*-set bits and 2 X- and 2 Y- high *Unit*-set bits. $\varepsilon = \sqrt{2} \times p$ corresponds to the distance between the centers of two strips displaced by one strip in X and one strip in Y. Taking into account the space resolution of a detector with strip segmentation, a Gaussian smearing is introduced on the reconstructed positions.

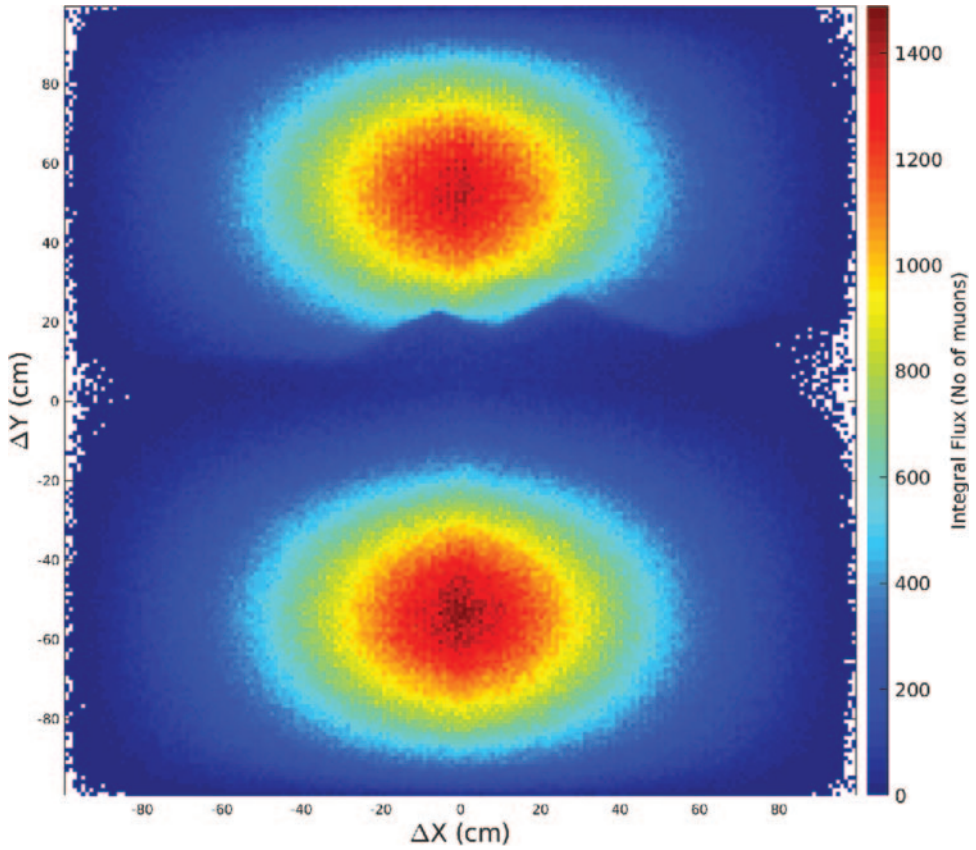

Fig. 6. – Integral of the muon flux acquired during the test phase (January-July 2017) at Nicolosi, studying the Monti Rossi. The ΔX and ΔY coordinates between the crossing point of the tracks in the external planes are expressed in cm, after multiplication of Δ in numbers of strips by strips width p.

The result of the test measurement campaign is shown in fig. 6, which reports the integral of the muon flux acquired. The common practice to express muography data as a function of X and Y displacement, ΔX and ΔY respectively, between entrance and exit coordinates of the muon tracks in the telescope external planes is followed. A muon coming from the front of the detector, *i.e.*, from the side pointed toward the object to be imaged, is identified by $\Delta Y > 0$ and vice versa. The tracks with the same $(\Delta X, \Delta Y)$, *i.e.*, parallel to the same direction, are grouped together. This convention reflects the assumption that the telescope is considered as a point compared to the target object.

3˙1. *Discussion of the results.* – In the upper part of fig. 6 ($\Delta Y > 0$) the profile of the Monti Rossi is clearly visible. The rise of muon counts as concentric rings is due to the convolution of telescope acceptance and muon flux dependence on zenith angle.

The muon flux coming from "open sky" ($\Delta Y < 0$), measured simultaneously to the flux attenuated by the target, was used to calculate the muon transmission, defined as the ratio of these two fluxes. The authors refer to [4] for a detailed definition of muon transmission. The plot of the measured muon transmission is shown in fig. 7(a).

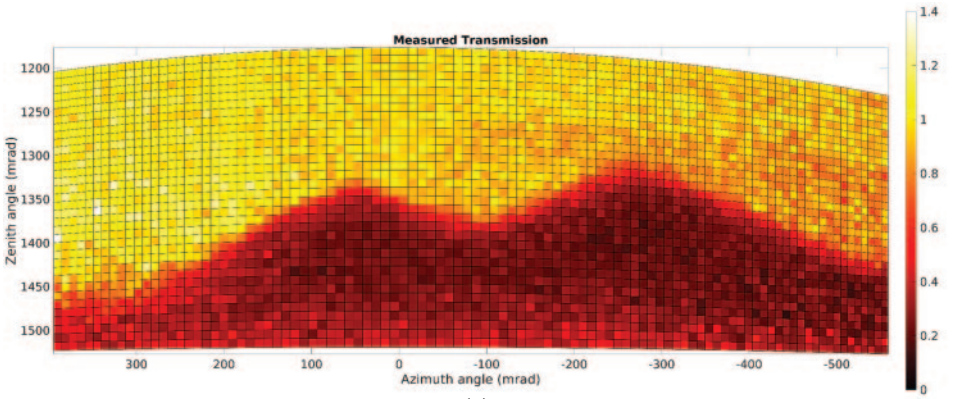

(a)

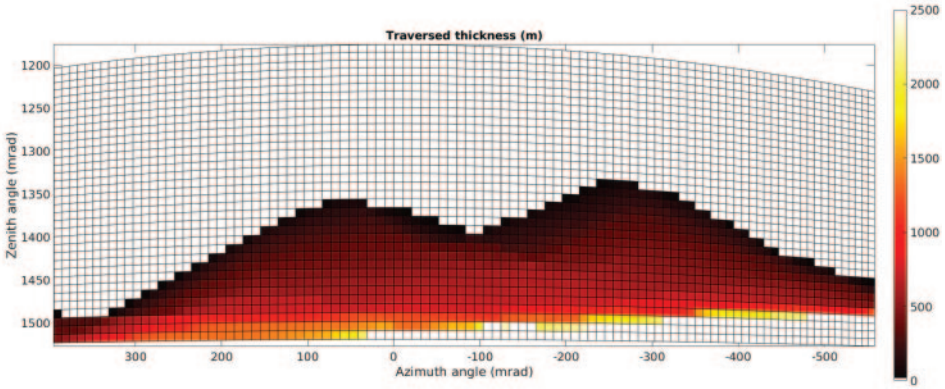

(b)

(c)

Fig. 7. – Comparison between measured muon transmission for each trajectory given by zenith and azimuth angles (a), traversed thickness calculated from DEM (b) and a photo of Monti Rossi from a point close to the installation site of the telescope (c). The trajectory with zenith angle = 0 and azimuth angle = 0 corresponds to the telescope axis.

Figure 7(b) shows the traversed thickness for each direction in the FOV of the telescope, in the same angular range considered for muon transmission, calculated from the Digital Elevation Model (DEM) already displayed in fig. 5. The comparison between figs. 7(a) and 7(b) shows that muon transmission decreases following down the profile of Monti Rossi, in a way similar to the increase of traversed thickness, as expected.

This trend is preserved until 50–70 mrad over the horizon where the muon transmission increases whereas the expected muon counts should be almost zero because the traversed thickness becomes very large. This is a drawback for all muography detectors which base the distinction of muon incoming direction only on the slope of the reconstructed trajectory. Between the possible candidates as noise source [14-16], there are "back-scattered" muons, *i.e.*, particles detected with upward-going trajectories after being scattered by the soil near the detector, as discussed by Jourde *et al.* [17]. These particles could enter the detector from the back and mimic the signal of penetrating muons with downward trajectories emerging from the target, leading to an incorrect reconstruction of their arrival direction. Back-scattered muons are considered the major responsible of noise in the range of 5° around the horizontal.

The bottom part of fig. 7 shows a picture of the Monti Rossi taken from a point near the telescope location during the test campaign. The target's view was covered by surrounding buildings from the exact location of the detector. Nevertheless, it is clearly visible that the shape of the crater is reproduced very well in the muographic image.

Regarding the Monti Rossi, we did not expect to observe strong density anomalies inside their volume and this led to successfully conclude the test phase after having solved all the technical issue related to data transmission to the cloud storage.

4. – Conclusions and outlooks

The results discussed in this paper confirm the positive conclusion of the test phase of the new muography detector developed by the MEV Collaboration. The mechanical structure proved to be relatively light and water tight in order to preserve the sensitive elements of the telescope and the electronics. All the problems regarding wireless communication with the detector were solved and the telescope is able to send data to cloud storage and independent from external power sources. The first muographic image of a geophysical target was acquired with a result consistent with the expectation. Hence, the telescope was transferred to the summit zone of the Etna Volcano (about 3100 m a.s.l.) at the beginning of August 2017. The detector acquired two set of data during the last part of summer of 2017 and from July to October 2018, before solar panels were covered by the snow.

In order to reject part of the background noise, a Time-of-Flight module between the outer matrices of the telescope was included at the end of the 2018 measurement campaign. The first data obtained with this system are under validation. In addition, an innovative Cherenkov-tag detector, based on silicon photomultiplier read-out, is under study to improve muography experiments by the correct assignment of particle arrival direction [18]. These solutions should allow to remove, in particular, near horizontal muons that may be wrongly reconstructed using tracking information only. However, because events identified as noise were tracked, they can be further studied to better comprehend background composition.

Soft muons, *i.e.*, muons with relatively low momenta, and other charged particles could strongly compromise muography reliability because they suffer large-angle scattering and mimic fake muon signals, respectively. As stated before, a fundamental

assumption for muography is that particles follow a straight track in traversing the target so that their trajectory can be back-projected in order to retrieve their path inside the object. The effects of background particles are an over-estimation of the muon flux, which results in an underestimated density of the target, and a blurring of the image with a loss of details. The last issue especially concerns very large targets which require the telescope to be placed far and nearly horizontal, *e.g.*, for the investigation of a volcano inner structure.

A well exploited passive solution is to include one or more slabs of absorber, especially made of high Z material as iron or lead. Depending on their thickness, they will introduce an energy cut-off for muons able to completely traverse the detector, while particles with energy slightly higher than the cut-off will be strongly deflected inside the telescope. Instead, hadrons and electrons (positrons) will be most likely stopped in the absorber. Then, a higher angular resolution is required in order to recognize scattering due to high Z material inside the detector, allowing to not discard these events. However, this solution imposes many mechanical constraints on detector construction and transportability which are not compatible with an installation in the summit zone of a tall volcano like Etna.

* * *

The construction of the telescope was funded by FIR2014 (Future in Research) and strongly supported by Parco dell'Etna National Park and INGV. Special thanks go to all the collaborators inside the MEV project, in particular to the principal investigator Prof. Domenico Lo Presti from the Department of Physics and Astronomy "E. Majorana" of the University of Catania.

REFERENCES

[1] Tanaka H. K. M. *et al.*, *Earth Planet. Sci. Lett.*, **263** (2007) 104.
[2] Lesparre N. *et al.*, *Geophys. J. Int.*, **190** (2012) 1008.
[3] Morishima K. *et al.*, *Nature*, **552** (2017) 386.
[4] Saracino G. *et al.*, *Sci. Rep.*, **7** (2017) 1181.
[5] Nishiyama R. *et al.*, *Geophys. Res. Lett.*, **44** (2017) 6244.
[6] Oláh L. *et al.*, *Sci. Rep.*, **8** (2018) 3207.
[7] Tanaka Hiroyuki K. M. *et al.*, *Philos. Trans. R. Soc. A: Math. Phys. Eng. Sci.*, **377** (2019) 20180143.
[8] Procureur S., *Nucl. Instrum. Methods Phys. Res. Sect. A:*, **878** (2018) 169.
[9] Lo Presti D. *et al.*, *Nucl. Instrum. Methods Phys. Res. Sect. A*, **904** (2018) 195.
[10] Riggi F. *et al.*, *Nucl. Instrum. Methods Phys. Res. Sect. A*, **912** (2018) 16.
[11] Gallo G. *et al.*, *J. Instrum.*, **11** (2016) C11014.
[12] Lesparre N. *et al.*, *Geophys. J. Int.*, **183** (2010) 1348.
[13] Ester M. *et al.*, *A density-based algorithm for discovering clusters in large spatial databases with noise* in *Proceedings of the Second International Conference on Knowledge Discovery and Data Mining (KDD-96), Portland, Oregon, USA* (AAAI Press) 1996, pp. 226–231.
[14] Nishiyama R. *et al.*, *Geophys. J. Int.*, **206** (2016) 1039.
[15] Oláh L. *et al.*, *Astropart. Phys.*, **93** (2017) 17.
[16] Gómez H. *et al.*, *J. Instrum.*, **12** (2017) P12018.
[17] Jourde K. *et al.*, *Geophys. Res. Lett.*, **40** (2013) 6334.
[18] Lo Presti D. *et al.*, *Sensors*, **19** (2019) 1183.